ISSN 0020-4412, Instruments and Experimental Techniques, 2010, Vol. 53, No. 2, pp. 165–171. © Pleiades Publishing, Ltd., 2010.
Original Russian Text © A.V. Sannikov, 2010, published in Pribory i Tekhnika Eksperimenta, 2010, No. 2, pp. 9–15.

NUCLEAR EXPERIMENTAL TECHNIQUES

Bismuth Activation Cross Sections for High Energy Neutrons

A. V. Sannikov

Institute for High Energy Physics, ul. Pobedy 1, Protvino, Moscow oblast, 142281 Russia
e-mail: sannikov@ihep.ru

Received July 16, 2009

Abstract—The bismuth activation cross sections were calculated within the scope of the generalized cascade model in the 15- to 1000-MeV range of neutron energies. These data were used in comparison with two experiments performed at the Institute for High Energy Physics and Rutherford Appleton Laboratory and in unfolding of high-energy neutron spectra from results of measurements. The equilibrium shape of the cascade peak in high-energy neutron spectra outside thick shields was confirmed.

DOI: 10.1134/S0020441210020028

INTRODUCTION

A number of innovative scientific and engineering programs, such as development of high-power neutron sources based on proton accelerators for material tests, electronuclear breeding, and transmutation of nuclear waste, have required that methods for high-energy neutron spectrometry be improved. It is difficult to measure neutron spectra at energies exceeding several tens of MeV, since most methods conventionally used to measure low-energy neutron spectra are inapplicable in this energy range. A carbon activation detector (CAD) based on the $^{12}C(n, x)^{11}C$ reaction with a 20-MeV threshold and an ~20-mb cross section over a wide energy range remains the sole widely used detector of high-energy neutrons.

A promising activation detector for this energy range is based on ^{209}Bi, for which the cross sections of the $^{209}Bi(n, xn)^{210-x}Bi$ ($x = 3–12$) reactions were measured in the energy range of 20–150 MeV [1]. These reactions have thresholds from 14.4 MeV ($x = 3$) to 88 MeV ($x = 12$) and sufficiently large cross sections—from 1700 to 40 mb as a maximum, respectively. The results of calculations performed according to the ALICE/89 code in [2] were in good agreement with the experimental data. Afterward, the author of this code revealed serious drawbacks of this model [3], which limited its usability by a range of nucleon energies below 100 MeV. In addition, results of measurements have significant errors (up to several tens of percent). In this connection, there is a necessity of determining the cross sections more precisely, particularly in the energy range of >100 MeV.

This paper is devoted to the theoretical investigation of the bismuth activation cross sections at neutron energies of 15–1000 MeV, which was performed within the scope of the generalized cascade model (GCM) [4, 5]. The results of this study are compared to the experimental data obtained by two independent research teams in high-energy neutron fields at the accelerator facilities of the Institute for High Energy Physics (IHEP) [6, 7] and the Rutherford Appleton Laboratory (RAL) [8, 9]. Neutron spectra were reconstructed by unfolding analysis of the measured rates of the $^{209}Bi(n, xn)$ and $^{12}C(n, x)^{11}C$ reactions.

CALCULATIONS OF THE BISMUTH ACTIVATION CROSS SECTIONS

The GCM is development of the cascade–exciton model of nuclear reactions used in the HADRON high-energy hadron transport code [10]. The main distinctive features of the GCM as compared with the previous models are as follows:

—a self-consistent model of the nuclear potential and the nucleon density in a nucleus, which is fully based on experimental data;

—description of nucleons by wave packets in the coordinate and momentum spaces, which allows the nonlocality of nucleon–nucleon interactions inside a nucleus to be taken into account;

—exact calculation of the classical trajectories of hadrons in the nuclear field; and

—taking into account the dependence of the nucleon–nucleon interaction cross sections on the nuclear matter density.

In [4], it was shown that the GCM agrees with an experiment in the total cross sections of nucleon–nucleus reactions at energies ranging from 10 MeV to 10 GeV without recourse to free parameters for individual nuclei. Expansion of the range of cascade model usability to the region of low energies has allowed us to exclude the preequilibrium nuclear reaction stage preceding the evaporation cascade. The successful description of double-differential cross sections for nucleon and complex particle production in nucleon–nucleus interactions at energies of <100 MeV [5] suggests that the spectrum of residual

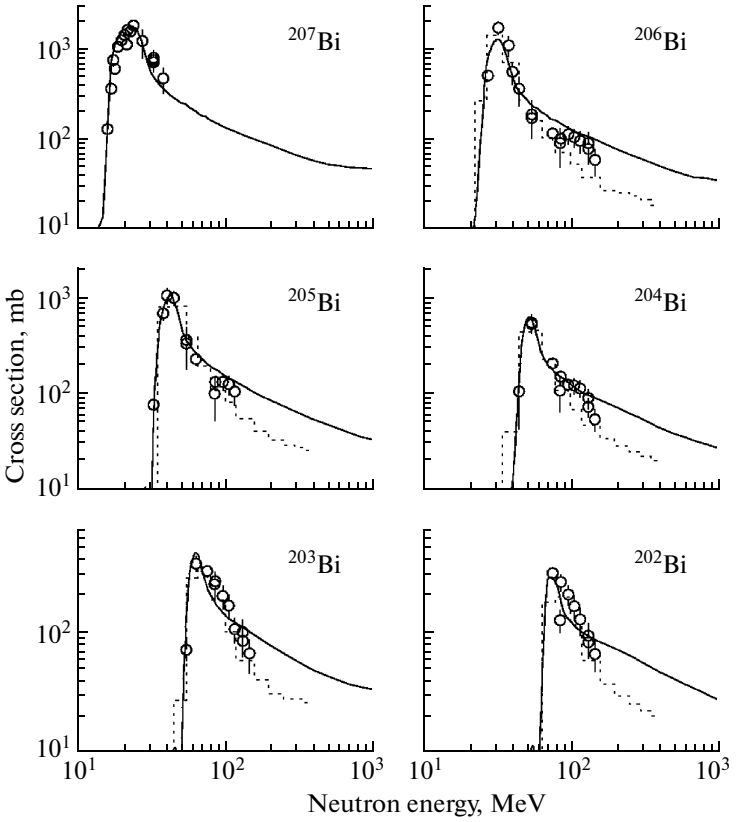

Fig. 1. ^{209}Bi$(n, xn)^{210-x}$Bi activation cross sections for neutrons with energies of 15–1000 MeV. The experimental data [1, 11] are shown with dots, the results of calculation in [2] are presented with histograms, and curves correspond to calculations according to the GCM (this paper).

nuclei can also be calculated with an adequate accuracy within the scope of the GCM.

The calculated activation cross sections of residual nuclei from ^{207}Bi to ^{202}Bi are presented in Fig. 1. This figure also shows experimental data [1] and [11] (for ^{207}Bi in the energy range of 16–24 MeV) and theoretical cross sections [2] given in [8]. In most cases, results of GCM calculations agree with the experiment within the limits of the errors; this conclusion is also valid for the theoretical data in [2]. Nevertheless, at energies of >100 MeV, the results of the two calculations systematically conflict with each other, the difference being as great as a factor of 3.

To test the energy dependences of the cross sections in the range of high energies, the proton activation cross sections for ^{209}Bi were calculated. In this case, the second production channel of bismuth isotopes appears, owing to the production of polonium isotopes undergoing β decay into bismuth nuclei with the same atomic weight. These reaction channels for the residual ^{207}Bi nucleus are shown in the schematic diagram presented below.

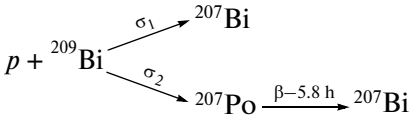

In such cases, independent and cumulative cross sections for nuclide production can be distinguished: $\sigma_{ind} = \sigma_1$ and $\sigma_{cum} = \sigma_1 + \nu_2\sigma_2$, where ν_2 is the relative probability of β decay of a polonium nucleus in comparison with α decay. In the cases described below, this probability is almost 100%.

The results of our calculation of the independent and cumulative cross sections for four nuclides are compared in Fig. 2 to the measured cumulative cross sections from the EXFOR database [12]. At proton energies near the reaction thresholds, the second channel dominates, since the ^{209}Bi$(p, pxn)^{209-x}$Bi reactions with proton escape are strongly suppressed by the high Coulomb barrier. At high energies, the independent cross sections are, on the contrary, close to cumulative ones; i.e., the cross sections of reactions with production of intermediate polonium nuclei are small. Our results generally are close to the experimental data in the energy range of >100 MeV, which is evidence in favor of the high-energy neutron cross sections calculated using the GCM (see Fig. 1).

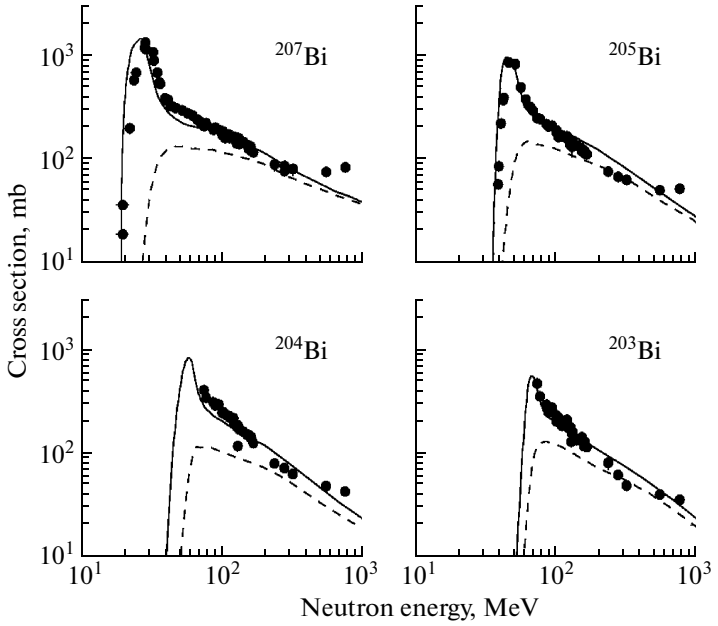

Fig. 2. Bismuth activation cross sections for protons with energies of 20–1000 MeV. The dots correspond to experimental cumulative cross sections [12]. GCM calculations: the independent and cumulative cross sections are presented with dashed and solid lines, respectively.

NEUTRON YIELD FROM THE SURFACE OF A TUNGSTEN TARGET IRRADIATED WITH ~1-GeV PROTONS

The experimental values of the ^{209}Bi(n, xn)$^{210-x}$Bi ($x = 3$–7) and ^{12}C(n, x)^{11}C reaction rates were presented in [6]. These values were measured near the surface of a cylindrical tungsten target with dimensions of ∅20 × 60 cm irradiated with 0.895- and 1.21-GeV protons at the U-1,5 accelerator at the IHEP. By reaction rate R_i is meant the probability of reaction i (the relative number of activated nuclei) when nuclei are irradiated with fluence Φ:

$$R_i = \int \sigma_i(E)\Phi(E)\mathrm{d}E, \qquad (1)$$

where σ_i is the microscopic cross section of reaction i. The activation detectors with dimensions of ∅20 × 1 mm (^{209}Bi) and ∅20 × 9 mm (CAD) were located at distances $Z = 2$, 8, 12, 17, 30, and 55 cm from the front end surface of the target. The proton beam intensity during measurements was ~10^{13} protons per cycle. The obtained experimental data were compared in [7] with results of calculations using the NMTC/JAERI, HERMES, and LAHET codes on the basis of the bismuth activation cross sections [2].

In this paper, the rates of the ^{209}Bi(n, xn)$^{210-x}$Bi reactions at the surface of a tungsten target were calculated with the aid of the HADRON code [10] using the neutron activation cross sections of bismuth, calculated according to the GCM. The profile of the proton beam incident on the tungsten target was specified based on the results of measurements in [6]. The results of calculations are compared in Fig. 3 to the experimental data. The latter were decreased by 11% for the ^{209}Bi(n, $6n$)^{204}Bi reaction in view of the state-of-the-art value of 375-keV photon yield taken from the NuDat 2.5 database in [13], which was 82%, as distinct from the yield of 73.7% accepted in [6]. Figure 3 also presents the results of calculations and measurements for the CAD; the calculations included the estimated cross sections of the ^{12}C(n, x)^{11}C reaction from [14, 15].

Comparison of the data in Fig. 3 showed that, first of all, the calculated values at $Z = 55$ cm were highly overestimated (3 to 4 times). Note that experimental data for ^{207}Bi nucleus at this distance are absent. A similar pattern was observed in the comparison of theoretical and experimental data in [7]. These discrepancies may be caused by incomplete representation of the experimental conditions in calculations (e.g., of the angular distribution of protons incident on the target). At smaller distances from the front target surface, results of calculations and measurements are in agreement within the limits of 20–30%, except for the ^{205}Bi nuclide at $Z = 30$ cm and an energy of 0.895 GeV.

To verify the calculated cross sections, neutron spectra at different distances were unfolded from the measured rates of nuclear reactions with bismuth and carbon. It is important that the CAD readings be taken into account in this task, since the bismuth activation cross sections are rather small at energies above 100 MeV, whereas the calculated neutron spectra shown in Fig. 4 stretch up to several hundreds of MeV. Hard neutron spectra are accompanied by a significant

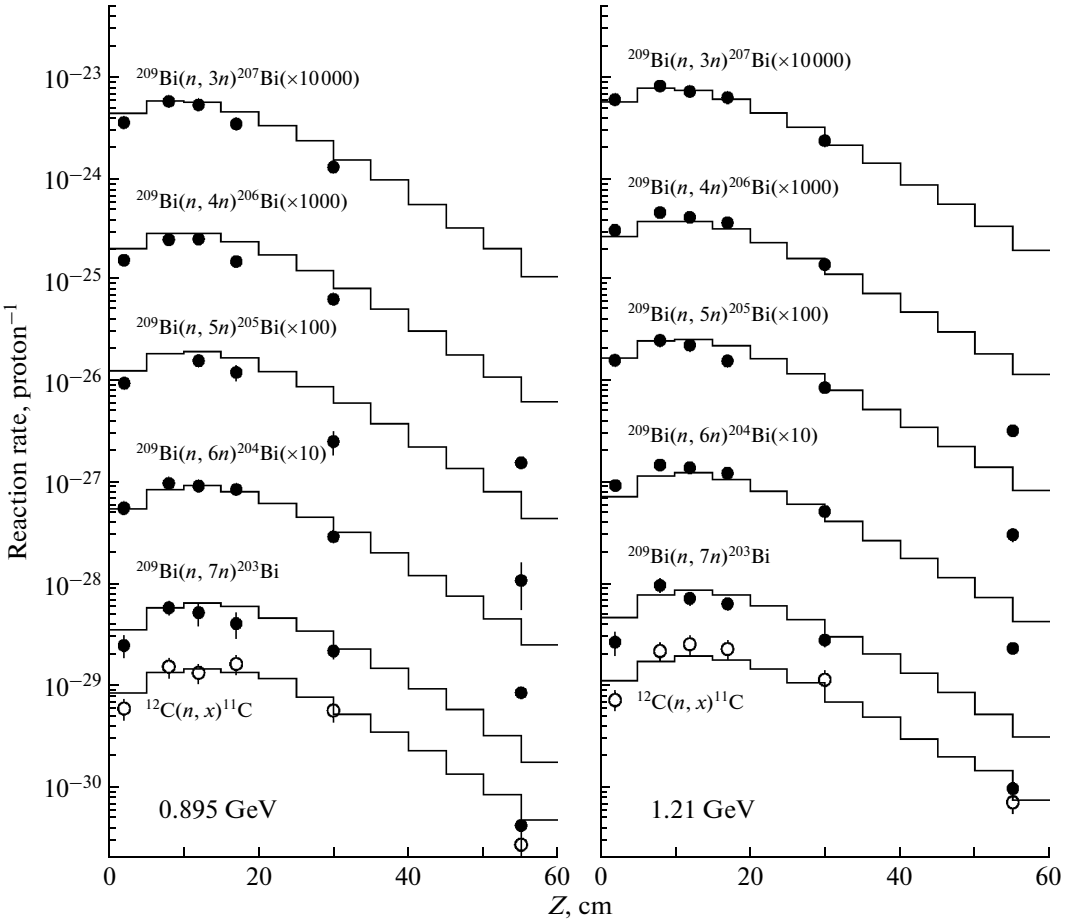

Fig. 3. ^{209}Bi(n, xn)$^{210-x}$Bi and ^{12}C(n, x)^{11}C reaction rates near the surface of the tungsten target during proton irradiation with energies of 0.895 and 1.210 GeV. The experimental data [6] are shown with dots, and the results of calculations are plotted as histograms.

component of charged hadrons (protons and pions), the contribution of which to the detector activation must be taken into account in neutron spectrum reconstruction.

The calculations using the HADRON code showed that this contribution to bismuth activation can be ignored, since the maxima of proton and pion spectra lie in the region much higher than 100 MeV, in which the cross sections for bismuth are small. For the carbon detector, the theoretical values of these contributions are presented in Table 1. They were subtracted from the CAD readings. The neutron spectra were unfolded using the BON95 code [15] based on the parameterization and iterations methods. The parameterization method was not used to perform this task, and the calculated neutron spectra acted as the initial approximations for the iteration procedure.

Table 1. Percentage contribution of charged hadrons to the CAD readings

Proton energy, GeV	Distance to the front end surface of the target, cm				
	2	8	12	17	30
0.895	2	4	5	8	12
1.210	2	5	7	9	14

The spectra were unfolded in 18 groups from 15.9 to 1000 MeV (ten groups per order of the neutron energy). The uncertainties in the activation cross sections for bismuth (Fig. 1) and carbon [14, 15], which were used in the reconstruction, were taken to be 15%. The test calculations showed that the errors of experimental data, which were 4–7% in the majority of cases, were too small, thus leading to considerable irregularities in reconstructed spectra. Therefore, the measurement errors were increased by 10% in order to obtain sufficiently smooth solutions, which was one of the main requirements in searching for a solution to incorrect reverse problems. At a proton energy of 0.895 MeV and distances of 8 and 30 cm, readings of the five detectors without ^{205}Bi were used in the reconstruction. In the first case, the experimental data are

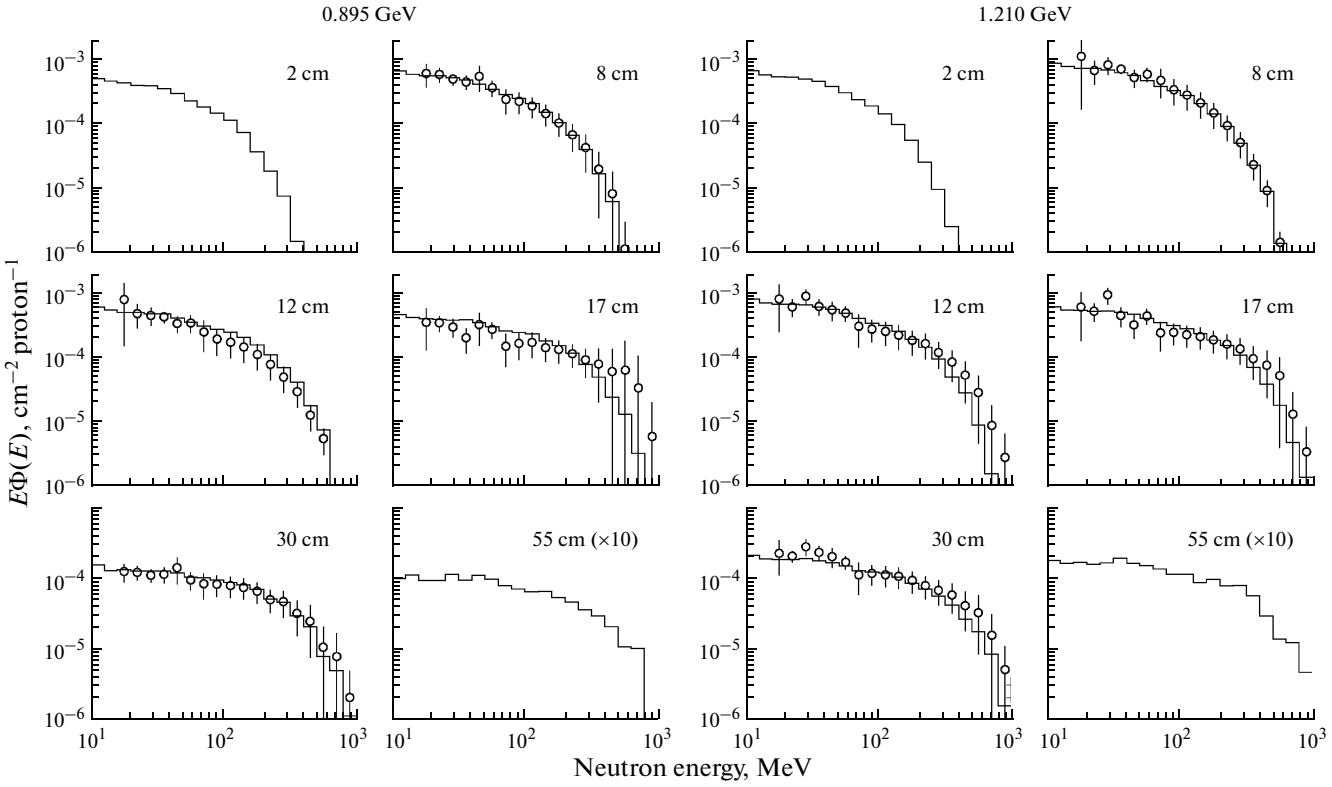

Fig. 4. Neutron spectra near the surface of the tungsten target at different distances from its front surface under exposure to protons with energies of 0.895 and 1.210 GeV. The histograms show the results of calculations, and the dots with errors are the results of unfolding from the readings of the bismuth detector and the CAD.

absent, while, in the second case, they apparently contain a nonexcluded systematic error.

The unfolded neutron spectra at four distances from the target's end surface and at two values of the proton energy are presented in Fig. 4 in comparison with the theoretical spectra. The experimental spectra generally agree with the computational data within the rms errors; although, irregularities are observed in some of the reconstructed spectra in spite of the increased measurement errors. The jumps in the spectrum for a distance of 17 cm at an energy of 0.895 MeV are most perceptible. In this case, the maximum deviation from the theoretical spectrum, primarily in the high-energy region, is also observed. It is our opinion that this deviation results from unaccounted systematic and/or random errors in the experimental data.

NEUTRON SPECTRA BEHIND THICK SHIELDS OF THE INTENSE SPALLATION NEUTRON SOURCE FACILITY

Experimental data on the rates of the ^{209}Bi(n, xn) ($x = 4$–10) reactions behind a thick shield of the intense spallation neutron source (ISNS) facility based on a 800-MeV proton accelerator at the RAL were presented in [8, 9]. A proton beam with a current of 170 μA bombarded a heavy-water-cooled tantalum target, thus generating a powerful neutron source at its surface. The measurements were performed at a point located above the target at an angle of 90° to the beam behind the combined steel (284 cm) and concrete (97 cm) shielding (point A). In the second set of measurements, the thickness of the concrete was increased by 60 cm (point B). Bismuth targets with dimensions of ∅8.0 × 1.1 cm and a CAD with dimensions of ∅8 × 3 cm were used in the measurements. The spectra from irradiated detectors were recorded and processed with a semiconductor spectrometer.

The results of measurements at points A and B are presented in Table 2. It is apparent that the measurement errors for bismuth are, as a rule, significantly higher than the errors in [6, 7]. At the same time, the errors for the CAD are considerably lower. This can be explained by the difference in the experimental techniques, as well as by the difference in the neutron flux density under the compared conditions. The neutron spectra were unfolded by the BON95 code in 16 groups with energies of 21.5 MeV (the ^{209}Bi(n, $4n$)^{206}Bi reaction threshold) and higher. The contribution of charged hadrons to the CAD readings was assumed to be 7.5% according to data [16]. The spectrum behind the top concrete shielding of the experimental hall of the U-70 proton synchrotron, which was also presented in [16], was used as an initial spectrum for the

Table 2. The $^{209}Bi(n, xn)^{210-x}Bi$ and $^{12}C(n, x)^{11}C$ reaction rates measured behind the thick shields of the intense neutron source at the RAL [8, 9]

Reaction	Reaction rate, 10^{-21} C^{-1}	
	point *A*	point *B*
$^{209}Bi(n, 4n)^{206}Bi$	100 ± 11.9%	28.6 ± 22.6%
$^{209}Bi(n, 5n)^{205}Bi$	91.8 ± 20.8%	26.0 ± 25.1%
$^{209}Bi(n, 6n)^{204}Bi$	53.1 ± 5.1%	16.3 ± 8.3%
$^{209}Bi(n, 7n)^{203}Bi$	44.0 ± 16.4%	14.0 ± 32.6%
$^{209}Bi(n, 8n)^{202}Bi$	27.4 ± 10.1%	9.33 ± 17.0%
$^{12}C(n, x)^{11}C$	6.75 ± 2.6%	2.04 ± 4.6%

iteration procedure. In Fig. 5, the reconstructed spectra at points *A* and *B* are compared to the data in [8, 9].

Except for the high-energy "tails," the shapes of the spectra unfolded using different programs and different cross sections are almost identical. As distinct from the smooth spectra obtained in our study, appreciable irregularities are observed in the spectra [8, 9], which points either to the inaccuracies of the bismuth and carbon activation cross sections used in the study or to the disadvantages of the spectrum reconstruction technique. One of the frequently occurring shortcomings consists in a failure to take the errors of the detector response functions into account. In our calculations, as was noted above, they were 15%. For the CAD, this error is predominant, since the experimental errors are 2.6 and 4.6% at points *A* and *B*, respectively (Table 2).

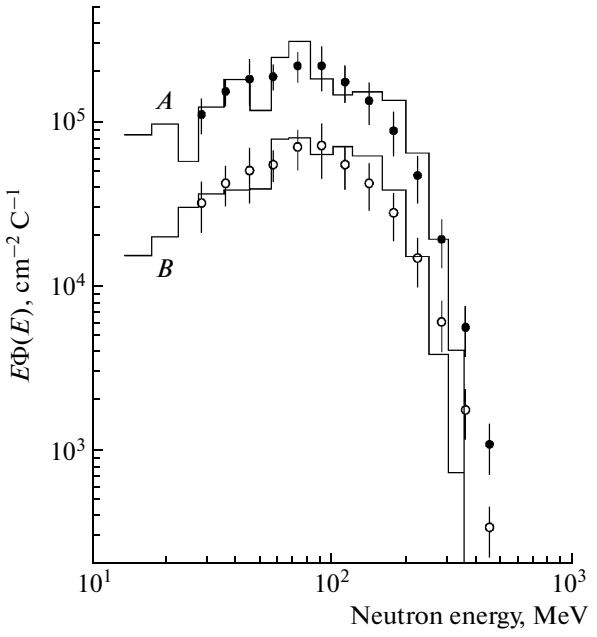

Fig. 5. Neutron spectra behind thick shields of the RAL ISNS at points *A* and *B*. The histograms correspond to data in [8, 9], and the dots show the results of this study.

Table 3. Integral characteristics of the cascade peaks in the neutron spectra behind the thick shields of the RAL ISNS

Point	$\dot{\Phi}$, 10^5 cm^{-2} C^{-1}	$\bar{E}$, MeV	$h^*(10)$, pSv cm^2
A	3.49 ± 0.30	87.3 ± 7.6	388 ± 11
B	1.06 ± 0.12	89.1 ± 8.3	383 ± 13

The data presented in Fig. 5 show that strengthening the thick shielding with a 60-cm concrete layer does not lead to a change in the neutron spectrum shape. This is one more piece of evidence that high-energy neutron spectra reach equilibrium behind thick shields or even behind relatively thin shields at large angles with the hadron beam incident on the target [15]. In this case, the characteristic shape of the cascade peak ($E > 20$ MeV) depends on the beam energy and the shield material (concrete, steel, or air in the case of neutron spectra generated by cosmic rays in the atmosphere) only slightly, as was shown in [15].

Table 3 contains the neutron flux densities per unit current of the proton beam, the average energies of the spectra, and the fluence to ambient dose equivalent conversion coefficients, which were determined from the unfolded neutron spectra with $E > 25$ MeV. Based on the measured flux densities at points *A* and *B*, it is possible to find attenuation length λ of a high-energy equilibrium neutron spectrum in a concrete shield, which is important for radiation protection. The attenuation length is determined from the expression

$$\Phi/\Phi_0 = r^{-2}\exp(-t/\lambda), \quad (2)$$

where t is the shield thickness and r is the distance from the target. In view of the concrete density of 2.36 g/cm^3 given in [8, 9], $\lambda = 55.5$ cm or 131 g/cm^2.

CONCLUSIONS

The bismuth activation cross sections calculated within the scope of the generalized cascade model do not generally contradict the data of two independent experiments and can be used in high-energy neutron spectrometry. The unfolded neutron spectra behind the shields with different thicknesses of the RAL ISNS confirm that the cascade peak in high-energy neutron spectra have an equilibrium shape, which was established earlier by calculation and used to reconstruct spectra behind the concrete and steel shields of the high-energy reference fields at CERN [14, 15], the neutron spectrum behind the top shield of the proton synchrotron at the IHEP [16], and the cosmic neutron spectrum at an altitude of 3 km [15, 17]. The attenuation length in concrete for neutrons of this equilibrium spectrum has been determined.

REFERENCES

1. Kim, E., Nakamura, T., Konno, A., et al., *Nucl. Sci. Eng.*, 1998, vol. 129, p. 209.
2. Fukahori, T., *Proc. 1991 Symp. Nuclear Data. Tokai, Japan, 1991*, JAERI-M 91-032, p. 106.
3. Blann, M., *Phys. Rev. C*, 1996, vol. 54, p. 1341.
4. Sannikov, A.V. and Savitskaya, E.N., *Radiat. Prot. Dosim.*, 2004, vol. 110, p. 27.
5. Sannikov, A.V. and Savitskaya, E.N., Abstracts of Papers, *IX Rossiiskaya nauchnaya konferentsiya "Radiatsionnaya zashchita i radiatsionnaya bezopasnost' v yadernykh tekhnologiyakh"* (IX Russ. Sci. Conf. on Radiation Protection and Radiation Safety in Nuclear Technologies), Obninsk, 2006, p. 276.
6. Krupnyi, G.I., Stetsenko, G.N., and Yanovich, A.A., *Preprint of Inst. for High Energy Phys.*, Protvino, 2000, no. 2000-34.
7. Takada, H., Meigo, S., Sasa, T., et al., *Proc. III Workshop on Simulating Accelerator Radiation Environments (SARE3)*, Tsukuba, Japan, 1997, p. 255.
8. Nunomiya, T., Nakao, N., Wright, P., et al., *KEK Report*, Tsukuba, 2001, no. 2001-24.
9. Nunomiya, T., Nakao, N., Wright, P., et al., *Nucl. Instrum. Methods Phys. Res. B*, 2001, vol. 179, p. 89.
10. Sannikov, A.V. and Savitskaya, E.N., *Nucl. Instrum. Methods Phys. Res. A*, 2000, vol. 450, p. 127.
11. Veeser, L.R., Arthur, E.D., and Young, P.G., *Phys. Rev. C*, 1977, vol. 16, p. 1792.
12. McLane, V., *National Nuclear Data Center (NNDC)*, Brookhaven National Laboratory, 1988; http://www.nndc.bnl.gov/
13. http://www.nndc.bnl.gov/nudat2/
14. Liu, J., Sannikov, A.V., and Stevenson, G.R., *CERN/TIS-RP/IR/94-17*, Geneva, 1994.
15. Sannikov, A.V., *Cand. Sci. (Phys.–Math.) Dissertation*, Protvino: Inst. for High Energy Phys., 2006.
16. Krupnyi, G.I., Peleshko, V.N., Rastsvetalov, Ya.N., et al., *Preprint of Inst. for High Energy Phys.*, Protvino, 2009, no. 2009-5.
17. Schraube, H., Jakes, J., Sannikov, A.V., et al., *Radiat. Prot. Dosim.*, 1997, vol. 70, p. 405.